Am J Cancer Res 2023;13(5):2104-2115
www.ajcr.us /ISSN:2156-6976/ajcr0149571

Brief Communication

Development and validation of immunogenic cell death-applied prediction model for esophageal carcinoma

Yazhou Wen[1*], Dongshan You[2*], Yongkang Bai[3], Jing Cao[2], Louqian Zhang[3], Xiaoyang Xia[2]

[1]Department of Anesthesiology, Women's Hospital of Nanjing Medical University, Nanjing Maternity and Child Health Care Hospital, Nanjing, Jiangsu, China; [2]Department of Medical Oncology, The Affiliated Chuzhou Hospital of Anhui Medical University/The First People's Hospital of Chuzhou, Chuzhou, Anhui, China; [3]Department of Thoracic Surgery, Nanjing Drum Tower Hospital, The Affiliated Hospital of Nanjing University Medical School, Nanjing, Jiangsu, China. [*]Equal contributors.

Received February 8, 2023; Accepted April 13, 2023; Epub May 15, 2023; Published May 30, 2023

Abstract: Evidence suggests that immunogenic cell death (ICD) releases cancer antigens that promote cytotoxic T-cell responses, potentially improving immunotherapy. However, the relationship between ICDs and esophageal cancer (EC) remains unclear. This study aimed to determine the role of ICDs in EC and to construct an ICD-based prognostic panel. RNA-seq data of EC and the corresponding clinical information were downloaded from the UCSC-Xena platform to explore the association between ICD gene expression and EC prognosis. The GSE53625 dataset was used to validate the proposed model. Differentially expressed genes (DEGs) between different molecular subtypes were identified to construct a new ICD-related prognosis panel and generate molecular subtypes using ConsensusClusterPlus. We created a prognostic profile based on the ICD and a nomogram based on the risk score. Compared with normal samples, ICD gene expression of malignant samples were significantly increased. 161 patients with EC were successfully divided into three subtypes (SubA, SubB, and SubC). Patients with EC in the SubC group had the best survival and lowest ICD score, whereas patients in the SubB group had the worst prognosis. DEGs between subtypes were evaluated, and risk panels were established using LASSO-Cox regression analysis. The prognosis of low-risk patients was significantly better than that of high-risk patients in both cohorts. The area under the curve of the receiver operating characteristic curve indicated that the risk group had a good prognostic value. Our study identified the molecular subtypes of EC and ICD-based prognostic signatures. Our three-gene risk panel could serve as a biomarker for effectively assessing the prognostic risk of patients with EC.

Keywords: Esophageal carcinoma, immunogenic cell death, biomarkers, clinical prognosis

Introduction

Esophageal cancer (EC), which occurs in the epithelial cells of the esophagus, is the sixth most common cause of cancer-related death worldwide [1]. The disease burden varied between countries and populations, mainly because of the prevalence of potential risk factors and subtype distribution. For example, China has the highest incidence of EC globally [2], but unlike Western countries, more than 90% of EC cases are squamous-cell carcinoma esophageal carcinoma (ESCC) [3]. Despite substantial improvements in ESCC treatment over the past 20 years, survival for EC remained low, with five-year survival rates ranging between 10-30% after diagnosis in most countries; the survival rates were 36%, 24%, and 30% in Japan [4], Australia [5], and China [6], respectively. Therefore, further improvement in the effectiveness, safety, and economy of EC therapy has become the focus of clinical medicine.

Immunogenic cell deaths (ICD) is a specific form of cell death that induces an immune response against the antigens of dying or dying cells [7]. ICD might activate danger signaling pathways mediated by surface calmodulin/heat shock proteins, secretion ATP, or HMGB1 [8]. ICD was an important predictor of solid anti-tumor

immunity [9, 10]. Conventional chemotherapy promotes T-cell-mediated destruction of residual cancer cells by inducing ICDs that convert malignant cells into vaccines and increase T-cell primers [11]. More importantly, cancer antigens released by ICDs were increasingly found to promote cytotoxic T cell responses, potentially improving immunotherapy [12, 13]. The main manifestation was that, when ICD occurs, numerous damage-related molecular patterns (DAMPs) were exposed and released, which made dying cancer cells have powerful adjuvant properties by attracting and activating antigen-presenting cells [14, 15]. Different innate immune receptors were involved in DAMPs-mediated ICD, and their synergies with DAMPs were required for ICD and anti-tumor immune responses [16]. However, the prognostic value and mechanism of ICD implantation in EC have not been thoroughly studied. Therefore, an in-depth understanding of the correlation between ICD-related genes and EC prognosis may provide a new method for the treatment and prognostic assessment of patients with EC.

In this study, RNA-seq data from the UCSC-Xena platform were used as the training cohort and the GSE53625 dataset was used as the validation cohort. The expression profile of ICD-related genes was obtained from a previous study (PMID: 27057433) and a molecular classifier of EC was successfully established. The relationships between molecular clustering, prognosis, immune cell infiltration, and ICD activity were investigated. Construction of risk panels using differentially expressed genes (DEGs) and clinical features of EC subtypes can be used as biomarkers to effectively assess the risk of prognosis in patients with EC.

Materials and methods

Data acquisition, differential expression analysis, and intersection identification

The RNA-seq data of EC were downloaded from the UCSC-Xena platform (https://xenabrowser.net/datapages/), along with clinical information (including age, sex, TNM stage, tumor stage, family history, lymph node examined count, neoplasm histologic grade, primary diagnosis, site of resection or biopsy, and disease type). Finally, 162 cancer samples and 11 normal samples with survival information were preserved [17]. In addition, GSE53625 dataset was downloaded from the GEO platform (http://www.ncbi.nlm.nih.gov/geo/), which included 179 EC and 179 normal samples as a validation cohort for a subsequent model [18]. The expression data downloaded above were normalized to log2 (FPKM + 1). We directly downloaded the processed and standardized probe expression matrix, and gene annotation information was obtained from the reference (PMID: 29317304). For different probes corresponding to the same gene symbol, the average value was used as the gene expression value for subsequent analyses. In total, 34 ICD-related genes (Table S1) were identified from the literature (PMID: 27057433) [19].

Cluster analysis

Univariate Cox regression analysis was used to screen the prognostic genes. ConsensusClusterPlus (v1.54 4.0) was used for consistent cluster analysis of ICD gene expression profile data. The proportional hazards assumption (PHA) was tested using the R survival package, which ensembled a test based on the weighted residuals. Heatmap clustering was performed using PheatMap (v1.0.12). The correlation between the cluster and clinical parameters is shown by overlaying diagrams and analyzed using the chi-square test. The four molecular subtypes of EC were evaluated using the R's GSVA package for ICD gene enrichment scores, and the Wilcoxon rank test was used to evaluate the differences in ICD gene enrichment scores among the different subtypes. Kaplan-Meier (KM) analysis was used to compare the prognoses of the four groups.

Cluster-based analysis of tumor immune microenvironment

To further explore the relationship between ICD subtypes and tumor microenvironment, the relative abundance of each immune cell in different subtypes was obtained using the "ESTIMATE" package of R, and Wilcoxon rank test was performed [20]. Simultaneously, using CIBERSORTx (https://cibersortx.stanford.edu/) online tools, based on gene expression data calculate the score 22 kinds of immune cells [21].

Identification of differentially expressed genes

The "limma" program was utilized to determine the DEGs among four subtypes, and the filtering threshold was *P* value < 0.05 [22].

Building the prognostic signature

Univariate Cox regression analysis was performed to identify the DEGs that were highly associated with prognosis in the training cohort. We used the prognostic genes to construct a prognostic model using LASSO Cox regression analysis via the lars package (Version 1.2) [23]. The genes whose regression coefficient was not 0 were included in the multivariate Cox analysis to construct the final prognostic risk scoring model. Based on the regression coefficient (c) derived from multivariate Cox regression analysis, the following formula was used to construct a prognostic signature: risk score = [c1 × expression level of gene (1)] + [c2 × expression level of gene (2)] + [cn × expression level of gene (n)]. Each patient was assigned a risk score using the following formula: The risk score for each patient was calculated according to the formula, and the "pROC" package of R software was used to draw the subject working characteristic curve to calculate the Yoden index to determine the optimal cut-off value of the risk score [24]. The median value divided the EC samples into high-risk and low-risk groups, and overall survival (OS) times were compared between the two groups using KM analysis. Time-related receiver operating characteristic (ROC) at 1, 3, and 5 years was performed using the timeROC package (v0.3) to evaluate the prognostic ability of the risk model. GSE53625 was selected as the external validation cohort from the GEO database.

Drug sensitivity prediction

Using the pharmacosensitivity genomics database, the "pRRophetic" package in R was used to estimate the sensitivity of chemotherapy agents in patients with EC [25]. The maximum inhibitory concentration of half (IC50) was calculated and quantified. The Wilcoxon test was used to compare differences in drug sensitivity between the high- and low-risk groups.

Results

Identification of ICD between EC and normal sample

First, we compared the distribution of ICD gene expression between EC and normal samples. As is shown in **Figure 1A**, the expression of ICD genes in EC samples differed from that in normal samples, and the expression of *PIK3CA* and *NT5E* in EC tissues was significantly higher than that in normal tissues ($P < 0.05$). However, correlation analysis of ICD gene expression showed that the expression of the ICD gene in normal samples had a certain correlation; however, with the occurrence of EC, the correlation of ICD gene expression was low (**Figure 1B**).

Identification of ICD-based molecular clusters in EC using consensus clustering analysis

To identify the ICD-based EC molecular clusters, 34 ICD-related genes were identified using consistent cluster analysis. Eighty percent of the samples and genes were selected from 10000 repeated sampling. K, denoting the maximum number of clusters, was set to ten. A hierarchical clustering algorithm and correlation distance matrix were used. According to the cumulative distribution function (CDF) curve and delta area, the optimal cluster number, K, was three, and three ICD-based EC molecular clusters were constructed (**Figure 2A-C**). To verify the rationality of the molecular subtypes of EC, ICD scores were calculated for the three molecular subtypes, and significant differences were observed in the ICD scores among the three molecular clusters ($P < 0.01$). The ICD score for SubC was the lowest (**Figure 2D**). Additionally, the three ICD-related clusters exhibited significantly different survival curves. Compared with other clusters, EC patients in the SubC cluster had the best survival, whereas those in the SubB cluster had the worst prognosis, indicating that ICD implantation had a protective effect on EC patients (**Figure 2E**). The genomic landscape of different patient clusters is shown in **Figure 2F**.

Cluster-based analysis of tumor immune microenvironment

The "ESTIMATE" R package was used to assess the differences in immune characteristics

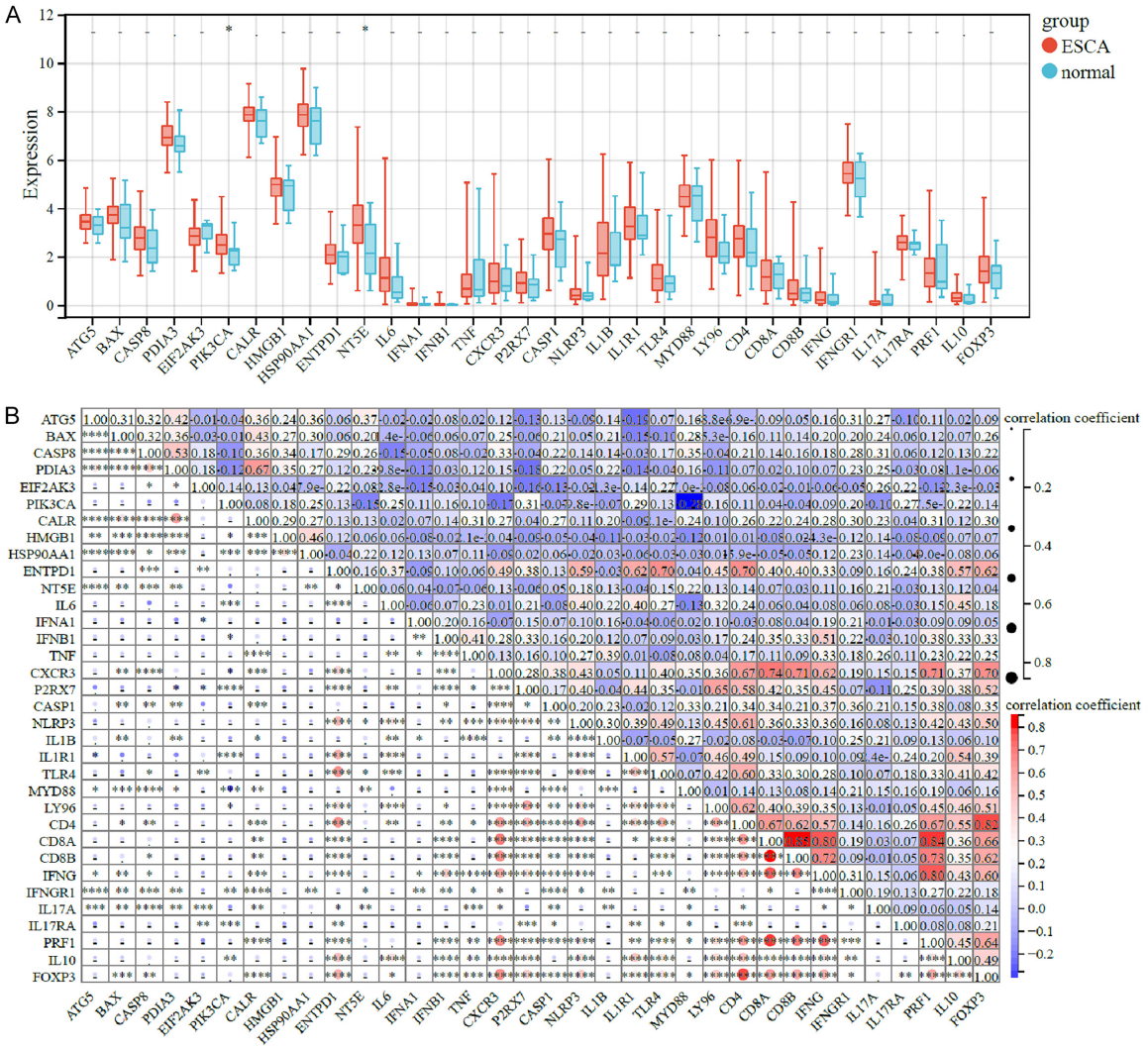

Figure 1. Role of immunogenic cell death in tumor and normal samples of esophageal cancer (EC). A. Difference in expression of ICD genes between tumor and normal samples in EC. B. Correlation analysis of ICD genes expression in esophageal carcinoma and normal samples.

among the three subtypes, including ImmuneScore, StromalScore, ESTIMATEScore, and Tumorpurity. As is shown in **Figure 3A**, the ImmuneScore, StromalScore, and ESTIMATEScore levels of the SubC subtype were lower than those of the other subtypes, but the tumor purity levels were enhanced. These results suggest that the prognosis of EC is negatively correlated with immune and stromal components. To further explore immune cells in the tumor distribution microenvironment, the CIBERSORTx online tool was used to calculate the percentage of different subtypes of 22 types of immune cell infiltration. Meanwhile, we found that naïve B cells, CD4 memory resting cells, CD8 T cells, CD4 memory activated cells, macrophages, and mast cells were significantly different among the three subtypes ($P < 0.05$; **Figure 3B**). Additionally, we analyzed the immune checkpoint and human leukocyte antigen (HLA) genes in the three clusters and found that all immune checkpoint genes, except for *VTCN1*, were downregulated in the SubC subtype, and the HLA genes in the SubC group showed the same trend (**Figure 3C**, **3D**, $P < 0.05$).

Risk model development of EC based on ICD-related genes and external verification

According to the thresholds described in the Methods section, a difference analysis was

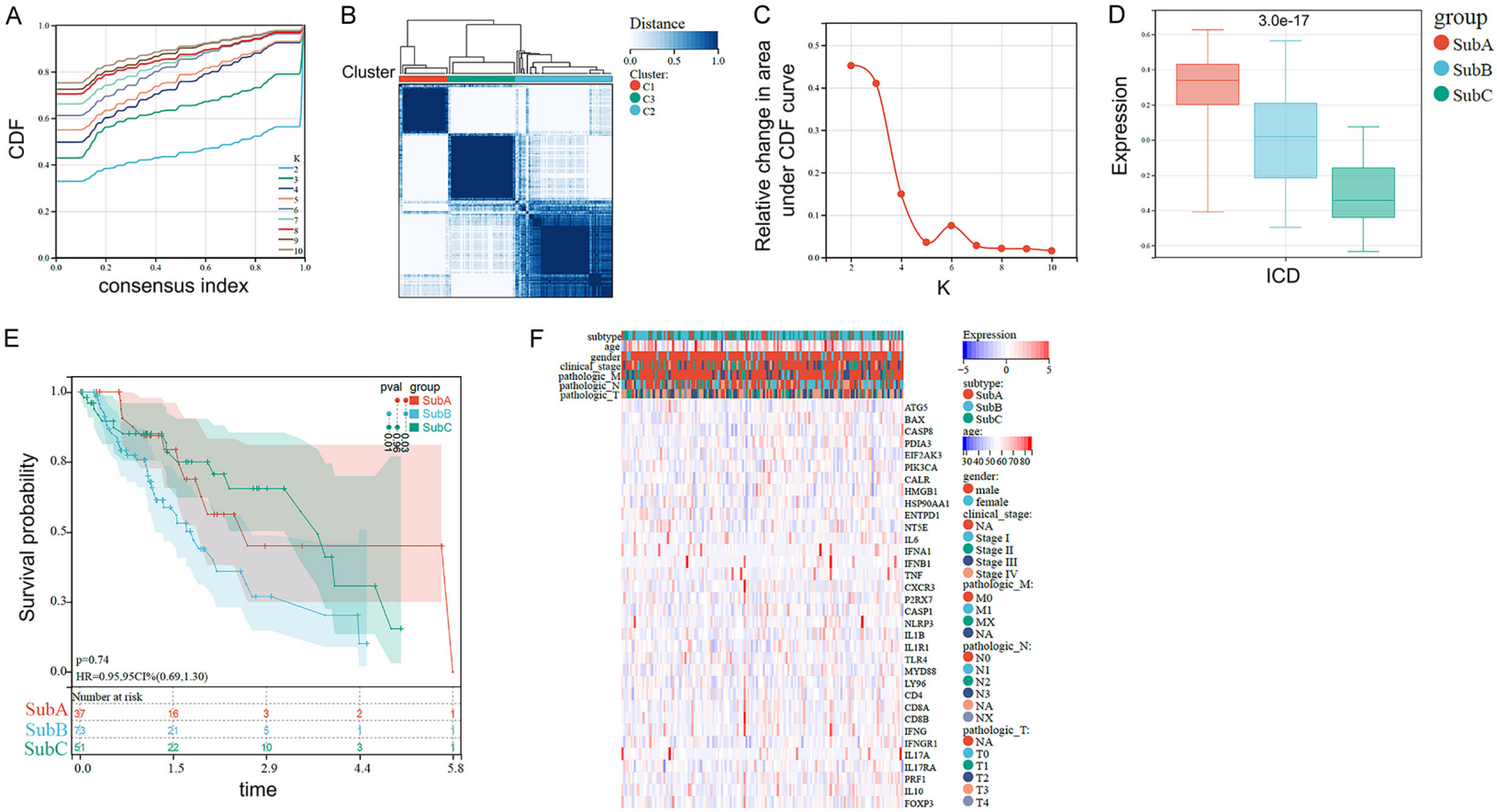

Figure 2. Consensus clustering of EC molecular subgroups based on immunogenic cell death (ICD). Cumulative distribution function curve (A), Consensus clustering matrix with K as 3 (B), and PAC verification curve (C). C1, C2, and C3 were SubA, SubB, and SubC, respectively. (D) ICD scores among three groups. (E) Kaplan-Meier survival curve of various clusters. (F) Distribution of clinical characteristics among various clusters.

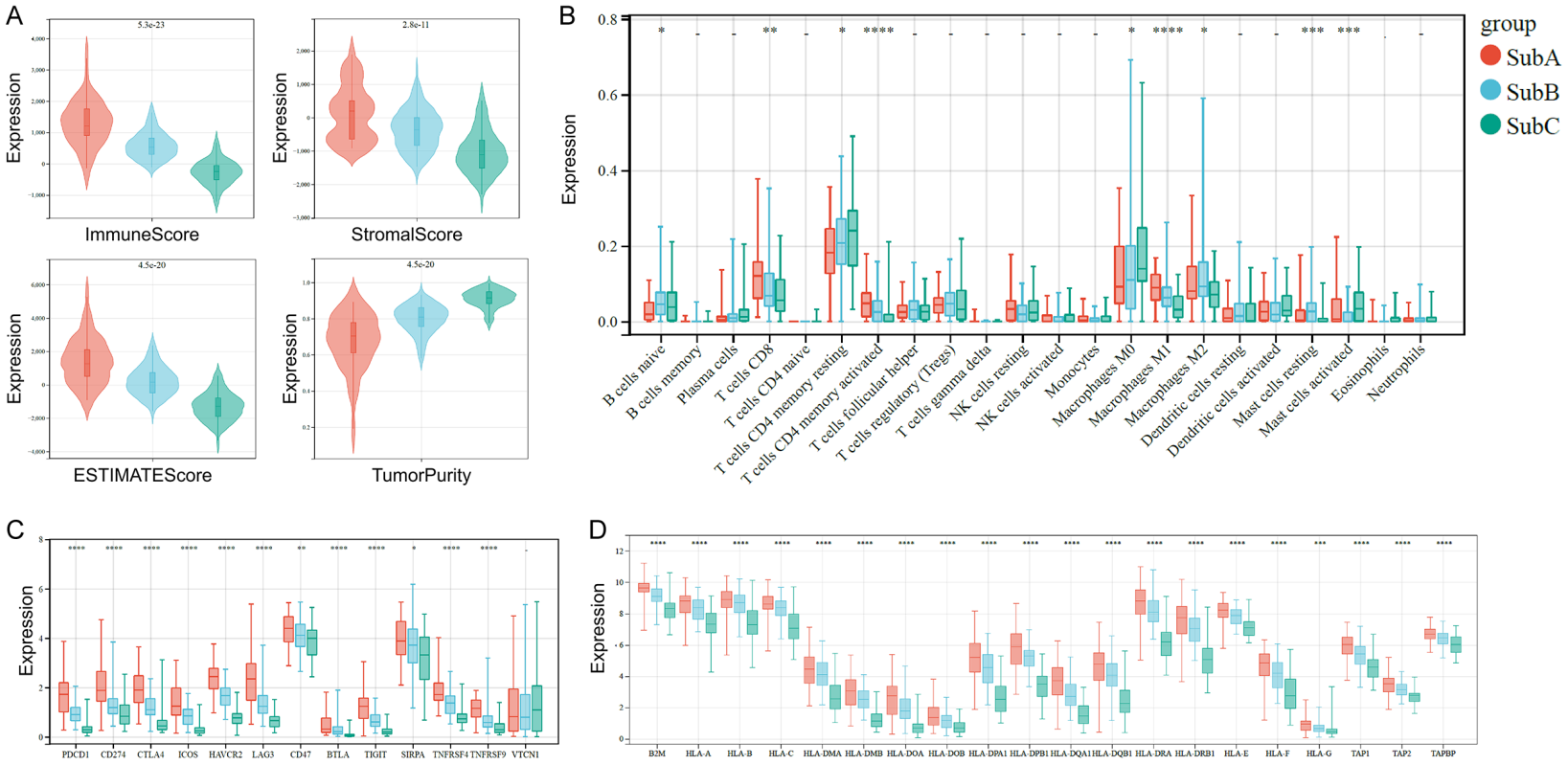

Figure 3. Cluster-based analysis of tumor immune microenvironment. A. Comparison of tumor immune microenvironment components. B. Box plots present differential immune infiltration. C. Immune checkpoint genes expression. D. Human leukocyte antigen family genes expression. $^{*}P < 0.05$. $^{**}P < 0.01$. $^{***}P < 0.001$. $^{****}P < 0.0001$.

performed for three subtypes: SubA and SubB, SubA and SubC, and SubB and SubC. For SubA and SubB, 3218 genes were identified, including 2052 up-regulated genes and 1166 down-regulated genes (Figure S1A). A total of 5455 genes were identified, including 4184 and 1271 up- and down-regulated genes, respectively (Figure S1B). A total of 4695 genes were identified, including 3762 and 933 up- and down-regulated genes, respectively (Figure S1C). A total of 1045 genes were obtained from the intersection of the three groups of differential genes (Figure S1D).

The DEG-based univariate Cox analysis of the three subtypes identified three prognostic genes (**Figure 4A**). LASSO regression analysis was performed on the prognostic genes identified using univariate Cox analysis. **Figure 4B** shows the loci of each independent variable. The number of independent variables approaching zero increased with increasing lambda (λ) value (**Figure 4C**).

The risk score of each patient was calculated, and the samples from the training and verification cohorts were divided into H (risk score higher than the median value of the risk score) and L (risk score lower than the median value of the risk score) groups (Figure S2). The KM curve showed that the prognosis of low-risk patients was significantly better than that of high-risk patients in both the training (P=1.3e-3, **Figure 4D**) and validation cohorts (P=6.0e-3, **Figure 4E**). The area under the curve (AUCs) of the time-dependent ROC curves for 1-, 3-, and 5-year OS was 0.77, 0.78, and 0.81, respectively (Figure S2C), indicating good predictive performance. A similar phenomenon was observed in the validation cohort; the ROC curves for the 1-, 3-, and 5-year OS rates were 0.65, 0.61, and 0.55, respectively (Figure S2D).

Developing a predictive nomogram for OS prediction

Data on risk scores and clinical features were analyzed using univariate and multivariate Cox regression analyses to determine prognostic factors. The results showed that risk scores and pathologic_N were significantly associated with prognosis ($P < 0.05$; **Figure 5A**, **5B**). A nomogram was established to accurately predict the clinical outcomes (**Figure 5C**). Simultaneously, the ROC curves of 1-, 3- and 5 years were 0.85, 0.83, and 0.80, respectively (**Figure 5D**). Based on the nomogram calibration map, the predicted OS results were closer to the observed results, and the calibration curves for 1 year showed good consistency; however, some deviation was observed over time (**Figure 5E**).

Cluster-based analysis of drug sensitivity

The drug sensitivity analysis showed that BIBW2992 (afatinib), bortezomib, Parthenolide, and RDEA119 (Refametinib) were expected to benefit the low-risk group (Figure S3).

Discussion

EC was found to be a common gastrointestinal tumor. Asian countries, such as Turkey, Kazakhstan, and China, have a high incidence of EC. Despite the prevalence of various treatments such as chemotherapy, targeted therapy, immunotherapy, and surgery, most patients diagnosed with EC will not benefit from surgery and show poor prognosis. Although some patients with EC are clinically cured by surgery, the tumor is prone to relapse and metastasis within a certain period following relevant chemotherapy and targeted drug therapy. Therefore, further improvements in the effectiveness, safety, and cost of EC therapy have become the focus of clinical medicine. To the best of our knowledge, this study is the first to identify molecular subtypes and prognostic signatures based on ICDs, which could help predict the clinical prognosis and therapeutic response in patients with EC.

In the anti-tumor process, in addition to the well-known cell death processes (such as apoptosis and pyroptosis), chemotherapy or radiotherapy has been employed in various types of cancer, which could induce specific cells to initiate the pro-inflammatory process, increase the activation of T cells, and develop a new therapeutic method that causes cell death (for example, ICD) [26]. Similarly, the results of the present study showed that ICD gene expression was higher in EC samples than in normal samples, suggesting that the cells in EC samples activated or enhanced the expression of immunogenic cell death genes to protect themselves and promote cell death.

After elucidating the protective effect of ICDs on EC, we performed cluster analysis and risk

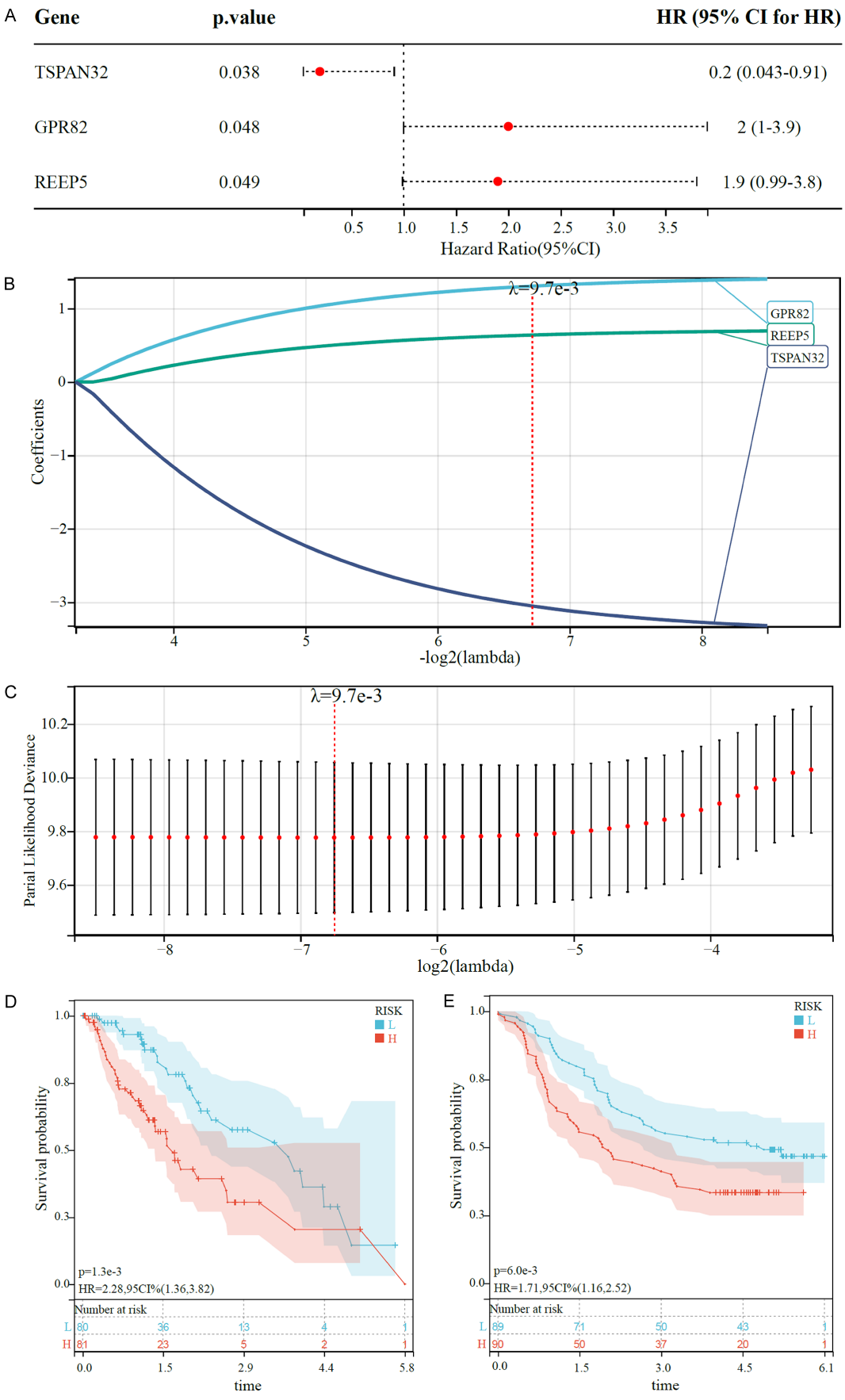
A
Gene
p.value
HR (95% CI for HR)
TSPAN32
0.038
0.2 (0.043-0.91)
GPR82
0.048
2 (1-3.9)
REEP5
0.049
1.9 (0.99-3.8)
0.5
1.0
1.5
2.0
2.5
3.0
3.5
Hazard Ratio(95%CI)
B
λ=9.7e-3
GPR82
REEP5
TSPAN32
Coefficients
-log2(lambda)
C
λ=9.7e-3
Parial Likelihood Deviance
log2(lambda)
D
RISK
L
H
Survival probability
p=1.3e-3
HR=2.28,95CI%(1.36,3.82)
Number at risk
L 80 36 13 4 1
H 81 23 5 2 1
time
E
RISK
L
H
Survival probability
p=6.0e-3
HR=1.71,95CI%(1.16,2.52)
Number at risk
L 89 71 50 43 1
H 90 50 37 20 1
time

Figure 4. Prognostic model of EC based on prognostic genes. (A) Univariate COX regression forest map. (B) LASSO coefficient profiles. (C) Plot of error rates from ten-fold cross-validation. KM survival curve illustrating the predictive value of risk model in the training (D) and validation (E) cohorts.

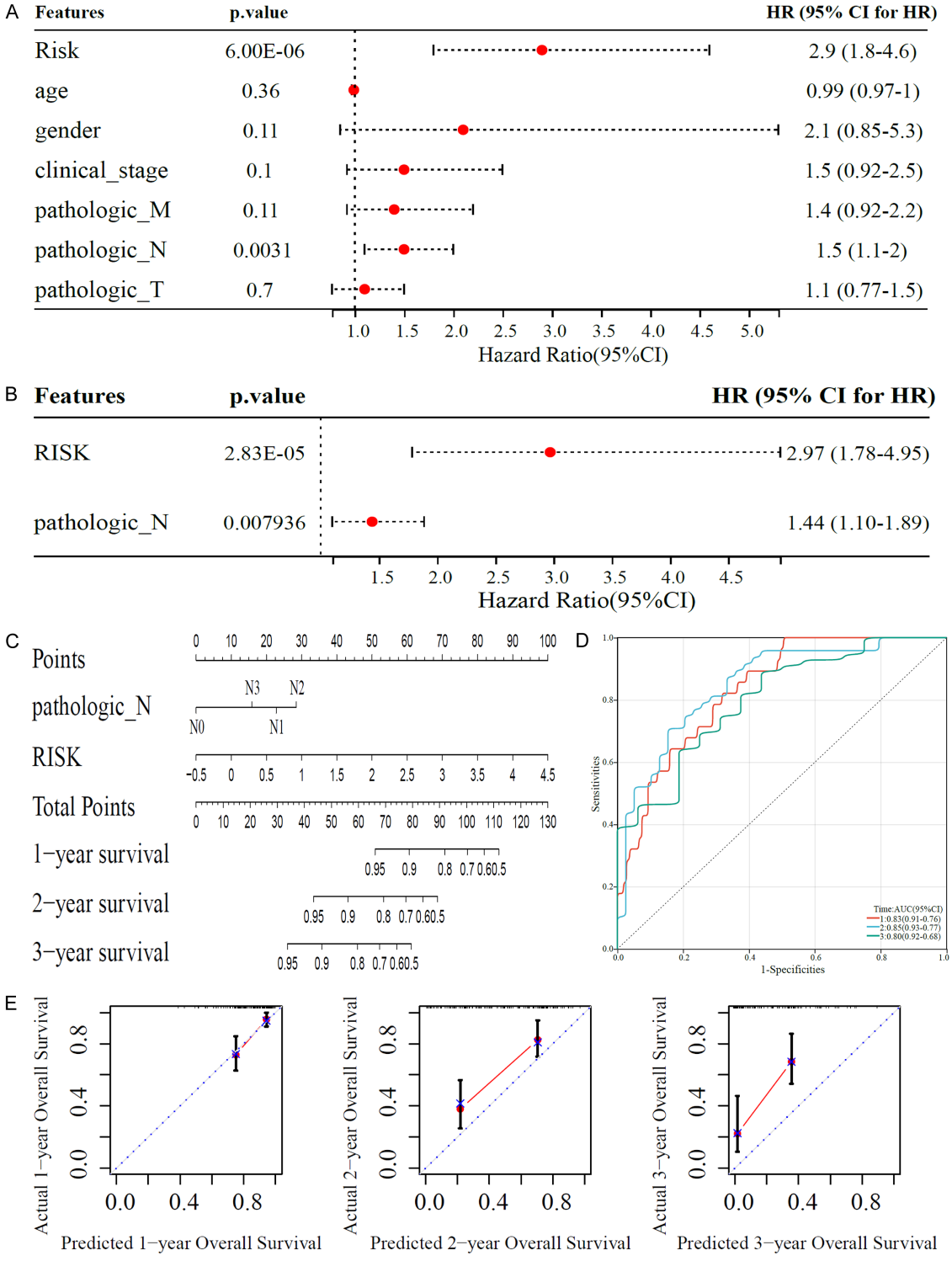

Figure 5. Construction of the nomogram for predicting OS of EC patients. Univariate (A) and multivariate (B) forest plots of the risk score model and clinicopathological characteristics associated with overall survival. (C) Nomogram was constructed based on two independent prognostic factors. (D) ROC curve. (E) Calibration plot for internal validation of the nomogram.

stratification to distinguish patients with EC with different ICD activities. First, 173 EC samples were genotyped according to ICD-related gene expression profiles, and three subtypes were identified. Patients with EC in the SubC group had the best survival and lowest ICD score, while the worst prognosis was observed in the SubB group. In addition, the SubC subtype had lower ImmuneScore, StromalScore, and ESTIMATEScore scores, but higher levels of tumor purity. These results consistently showed that the lower the ICD score, the better the clinical outcome of the SubC subtype, which also verified the protective effect of ICDs on EC.

To explore the potential prognostic mechanisms of the proposed ICD-based molecular subtypes and the causes of prognostic differences among the different subtypes, we compared the tumor immune microenvironments of the different subtypes. Interestingly, we found significantly higher levels of CD4+ T cells and M0 macrophages, and lower levels of immune checkpoint gene expression in patients in the SubC group with low ICD scores and good clinical outcomes. CD8+ T cells are an important component of tumor-infiltrating lymphocytes, which are manifested by the host's immune response to cancer cells [27]. CD8+ T cell infiltration could be used as a predictive marker [28]. As a major effector of humoral immunity, B cells stimulate T cell responses by producing immunoglobulins and prevent tumor progression by directly destroying tumor cells [29]. Therefore, high infiltration of immune cells is closely related to good prognosis of EC.

The R kit was used for univariate Cox regression analysis, resulting in the screening of three genes with significant prognostic correlation, and the prognostic model of EC patients was established using LASSO Cox analysis. Patients were divided into high- and low-risk groups based on their risk scores. We found that the prognosis of EC patients in the low-risk group was better than that of patients in the high-risk group. The ROC curve showed good predictive performance. Similar results have been reported in previous studies. Xu et al. developed an immune-related genes to predict prognosis in patients with osteosarcoma [30]. Another prognostic feature based on circulating nucleosomes and immunogenic cell death markers predicted the prognosis of pancreatic cancer [31]. The present study also examined correlations between prognostic risk scores, patient characteristics, and prognosis. Risk scores and pathological N were independent prognostic factors for OS. Overall, although the effectiveness of the prognostic models is slightly worse than that of similar studies [32, 33], the ICD markers in the present study were of great value for the prognosis of patients with EC.

In the present study, patients in the low-risk group may have benefitted from fuel-based drugs. Among them, BIBW2992 (Afatinib) is an EGFR inhibitor, which was approved for use in non-small cell lung cancer with EGFR mutations; Bortezomib was a proteasome inhibitor, and patients with mantle cell lymphoma or multiple myeloma were approved to be treated with it; Parthenolide was a HDAC1 inhibitor and RDEA119 (Refametinib) was an MEK 1/2 inhibitor, both of which have not obtained clinical indications for treating tumors. These four drugs have not yet been approved for clinical use in EC, and further research is needed to explore their correlation with ICD expression.

The results presented here should be considered exploratory rather than conclusive because this study was a retrospective analysis of the data from publicly accessible sources. Further in vitro and in vivo experiments, and prospective studies, are required to validate the findings. Nonetheless, the results can aid the development of new biomarkers for patients with EC.

Conclusion

Overall, we identified molecular subtypes of EC-based ICDs and used them to construct prognostic signatures. Different molecular subtypes and risk groups were analyzed for clinical characteristics, tumor immune microenvironment, and survival. In future, the proposed signatures may provide clinical evidence to support decisions regarding the treatment and prognosis of patients with EC.

Disclosure of conflict of interest

None.

Address correspondence to: Xiaoyang Xia, Department of Medical Oncology, The Affiliated Chuzhou Hospital of Anhui Medical University/The First

People's Hospital of Chuzhou, Chuzhou, Anhui, China. E-mail: xiaxiaoyang9@163.com; Louqian Zhang, Department of Thoracic Surgery, Nanjing Drum Tower Hospital, The Affiliated Hospital of Nanjing University Medical School, Nanjing, Jiangsu, China. E-mail: zhanglouqian@126.com

References

[1] Sung H, Ferlay J, Siegel RL, Laversanne M, Soerjomataram I, Jemal A and Bray F. Global cancer statistics 2020: GLOBOCAN estimates of incidence and mortality worldwide for 36 cancers in 185 countries. CA Cancer J Clin 2021; 71: 209-249.

[2] Bray F, Ferlay J, Soerjomataram I, Siegel RL, Torre LA and Jemal A. Global cancer statistics 2018: GLOBOCAN estimates of incidence and mortality worldwide for 36 cancers in 185 countries. CA Cancer J Clin 2018; 68: 394-424.

[3] Abnet CC, Arnold M and Wei WQ. Epidemiology of esophageal squamous cell carcinoma. Gastroenterology 2018; 154: 360-373.

[4] Allemani C, Matsuda T, Di Carlo V, Harewood R, Matz M, Nikšić M, Bonaventure A, Valkov M, Johnson CJ, Estève J, Ogunbiyi OJ, Azevedo E Silva G, Chen WQ, Eser S, Engholm G, Stiller CA, Monnereau A, Woods RR, Visser O, Lim GH, Aitken J, Weir HK and Coleman MP; CONCORD Working Group. Global surveillance of trends in cancer survival 2000-14 (CONCORD-3): analysis of individual records for 37,513,025 patients diagnosed with one of 18 cancers from 322 population-based registries in 71 countries. Lancet 2018; 391: 1023-1075.

[5] Arnold M, Rutherford MJ, Bardot A, Ferlay J, Andersson TM, Myklebust TÅ, Tervonen H, Thursfield V, Ransom D, Shack L, Woods RR, Turner D, Leonfellner S, Ryan S, Saint-Jacques N, De P, McClure C, Ramanakumar AV, Stuart-Panko H, Engholm G, Walsh PM, Jackson C, Vernon S, Morgan E, Gavin A, Morrison DS, Huws DW, Porter G, Butler J, Bryant H, Currow DC, Hiom S, Parkin DM, Sasieni P, Lambert PC, Møller B, Soerjomataram I and Bray F. Progress in cancer survival, mortality, and incidence in seven high-income countries 1995-2014 (ICBP SURVMARK-2): a population-based study. Lancet Oncol 2019; 20: 1493-1505.

[6] Zeng H, Chen W, Zheng R, Zhang S, Ji JS, Zou X, Xia C, Sun K, Yang Z, Li H, Wang N, Han R, Liu S, Li H, Mu H, He Y, Xu Y, Fu Z, Zhou Y, Jiang J, Yang Y, Chen J, Wei K, Fan D, Wang J, Fu F, Zhao D, Song G, Chen J, Jiang C, Zhou X, Gu X, Jin F, Li Q, Li Y, Wu T, Yan C, Dong J, Hua Z, Baade P, Bray F, Jemal A, Yu XQ and He J. Changing cancer survival in China during 2003-15: a pooled analysis of 17 population-based cancer registries. Lancet Glob Health 2018; 6: e555-e567.

[7] Galluzzi L, Buqué A, Kepp O, Zitvogel L and Kroemer G. Immunogenic cell death in cancer and infectious disease. Nat Rev Immunol 2017; 17: 97-111.

[8] Garg AD, Krysko DV, Verfaillie T, Kaczmarek A, Ferreira GB, Marysael T, Rubio N, Firczuk M, Mathieu C, Roebroek AJ, Annaert W, Golab J, de Witte P, Vandenabeele P and Agostinis P. A novel pathway combining calreticulin exposure and ATP secretion in immunogenic cancer cell death. EMBO J 2012; 31: 1062-79.

[9] Kepp O, Senovilla L, Vitale I, Vacchelli E, Adjemian S, Agostinis P, Apetoh L, Aranda F, Barnaba V, Bloy N, Bracci L, Breckpot K, Brough D, Buqué A, Castro MG, Cirone M, Colombo MI, Cremer I, Demaria S, Dini L, Eliopoulos AG, Faggioni A, Formenti SC, Fučíková J, Gabriele L, Gaipl US, Galon J, Garg A, Ghiringhelli F, Giese NA, Guo ZS, Hemminki A, Herrmann M, Hodge JW, Holdenrieder S, Honeychurch J, Hu HM, Huang X, Illidge TM, Kono K, Korbelik M, Krysko DV, Loi S, Lowenstein PR, Lugli E, Ma Y, Madeo F, Manfredi AA, Martins I, Mavilio D, Menger L, Merendino N, Michaud M, Mignot G, Mossman KL, Multhoff G, Oehler R, Palombo F, Panaretakis T, Pol J, Proietti E, Ricci JE, Riganti C, Rovere-Querini P, Rubartelli A, Sistigu A, Smyth MJ, Sonnemann J, Spisek R, Stagg J, Sukkurwala AQ, Tartour E, Thorburn A, Thorne SH, Vandenabeele P, Velotti F, Workenhe ST, Yang H, Zong WX, Zitvogel L, Kroemer G and Galluzzi L. Consensus guidelines for the detection of immunogenic cell death. Oncoimmunology 2014; 3: e955691.

[10] Dudek-Perić AM, Ferreira GB, Muchowicz A, Wouters J, Prada N, Martin S, Kiviluoto S, Winiarska M, Boon L, Mathieu C, van den Oord J, Stas M, Gougeon ML, Golab J, Garg AD and Agostinis P. Antitumor immunity triggered by melphalan is potentiated by melanoma cell surface-associated calreticulin. Cancer Res 2015; 75: 1603-14.

[11] Garg AD, More S, Rufo N, Mece O, Sassano ML, Agostinis P, Zitvogel L, Kroemer G and Galluzzi L. Trial watch: immunogenic cell death induction by anticancer chemotherapeutics. Oncoimmunology 2017; 6: e1386829.

[12] Apetoh L, Ghiringhelli F, Tesniere A, Obeid M, Ortiz C, Criollo A, Mignot G, Maiuri MC, Ullrich E, Saulnier P, Yang H, Amigorena S, Ryffel B, Barrat FJ, Saftig P, Levi F, Lidereau R, Nogues C, Mira JP, Chompret A, Joulin V, Clavel-Chapelon F, Bourhis J, André F, Delaloge S, Tursz T, Kroemer G and Zitvogel L. Toll-like receptor 4-dependent contribution of the im-

mune system to anticancer chemotherapy and radiotherapy. Nat Med 2007; 13: 1050-9.
[13] Zitvogel L, Apetoh L, Ghiringhelli F and Kroemer G. Immunological aspects of cancer chemotherapy. Nat Rev Immunol 2008; 8: 59-73.
[14] Fucikova J, Kepp O, Kasikova L, Petroni G, Yamazaki T, Liu P, Zhao L, Spisek R, Kroemer G and Galluzzi L. Detection of immunogenic cell death and its relevance for cancer therapy. Cell Death Dis 2020; 11: 1013.
[15] Ahmed A and Tait SWG. Targeting immunogenic cell death in cancer. Mol Oncol 2020; 14: 2994-3006.
[16] Gong T, Liu L, Jiang W and Zhou R. DAMP-sensing receptors in sterile inflammation and inflammatory diseases. Nat Rev Immunol 2020; 20: 95-112.
[17] Goldman MJ, Craft B, Hastie M, Repečka K, McDade F, Kamath A, Banerjee A, Luo Y, Rogers D, Brooks AN, Zhu J and Haussler D. Visualizing and interpreting cancer genomics data via the Xena platform. Nat Biotechnol 2020; 38: 675-678.
[18] Barrett T, Wilhite SE, Ledoux P, Evangelista C, Kim IF, Tomashevsky M, Marshall KA, Phillippy KH, Sherman PM, Holko M, Yefanov A, Lee H, Zhang N, Robertson CL, Serova N, Davis S and Soboleva A. NCBI GEO: archive for functional genomics data sets--update. Nucleic Acids Res 2013; 41: D991-5.
[19] Garg AD, De Ruysscher D and Agostinis P. Immunological metagene signatures derived from immunogenic cancer cell death associate with improved survival of patients with lung, breast or ovarian malignancies: a large-scale meta-analysis. Oncoimmunology 2016; 5: e1069938.
[20] Available from: https://CRAN.R-project.org/package=estimatr.
[21] Steen CB, Liu CL, Alizadeh AA and Newman AM. Profiling cell type abundance and expression in bulk tissues with CIBERSORTx. Methods Mol Biol 2020; 2117: 135-157.
[22] Ritchie ME, Phipson B, Wu D, Hu Y, Law CW, Shi W and Smyth GK. limma powers differential expression analyses for RNA-sequencing and microarray studies. Nucleic Acids Res 2015; 43: e47.
[23] Friedman J, Hastie T and Tibshirani R. Regularization paths for generalized linear models via coordinate descent. J Stat Softw 2010; 33: 1-22.
[24] Robin X, Turck N, Hainard A, Tiberti N, Lisacek F, Sanchez JC and Müller M. pROC: an open-source package for R and S+ to analyze and compare ROC curves. BMC Bioinformatics 2011; 12: 77.
[25] Geeleher P, Cox N and Huang RS. pRRophetic: an R package for prediction of clinical chemotherapeutic response from tumor gene expression levels. PLoS One 2014; 9: e107468.
[26] Land WG. The role of damage-associated molecular patterns (DAMPs) in human diseases: part II: DAMPs as diagnostics, prognostics and therapeutics in clinical medicine. Sultan Qaboos Univ Med J 2015; 15: e157-70.
[27] Gajewski TF, Schreiber H and Fu YX. Innate and adaptive immune cells in the tumor microenvironment. Nat Immunol 2013; 14: 1014-22.
[28] Lee J, Kim B, Jung HA, La Choi Y and Sun JM. Nivolumab for esophageal squamous cell carcinoma and the predictive role of PD-L1 or CD8 expression in its therapeutic effect. Cancer Immunol Immunother 2021; 70: 1203-1211.
[29] Tokunaga R, Naseem M, Lo JH, Battaglin F, Soni S, Puccini A, Berger MD, Zhang W, Baba H and Lenz HJ. B cell and B cell-related pathways for novel cancer treatments. Cancer Treat Rev 2019; 73: 10-19.
[30] Yang J, Zhang J, Na S, Wang Z, Li H, Su Y, Ji L, Tang X, Yang J and Xu L. Integration of single-cell RNA sequencing and bulk RNA sequencing to reveal an immunogenic cell death-related 5-gene panel as a prognostic model for osteosarcoma. Front Immunol 2022; 13: 994034.
[31] Wittwer C, Boeck S, Heinemann V, Haas M, Stieber P, Nagel D and Holdenrieder S. Circulating nucleosomes and immunogenic cell death markers HMGB1, sRAGE and DNAse in patients with advanced pancreatic cancer undergoing chemotherapy. Int J Cancer 2013; 133: 2619-30.
[32] Wang M, Jiang F, Wei K, Mao E, Yin G and Wu C. Identification of novel gene signature associated with cell glycolysis to predict survival in hepatocellular carcinoma patients. J Oncol 2021; 2021: 5564525.
[33] Mao Y, Hu Z, Xu X, Xu J, Wu C, Jiang F and Zhou G. Identification of a prognostic model based on costimulatory molecule-related subtypes and characterization of tumor microenvironment infiltration in acute myeloid leukemia. Front Genet 2022; 13: 973319.

Table S1. ICD genes list

ATG5
BAX
CASP8
PDIA3
EIF2AK3
PIK3CA
CALR
HMGB1
HSP90AA1
ENTPD1
NT5E
IL6
IFNA1
IFNB1
TNF
CXCR3
P2RX7
CASP1
NLRP3
IL1B
IL1R1
TLR4
MYD88
LY96
CD4
CD8A
CD8B
IFNG
IFNGR1
IL17A
IL17RA
PRF1
IL10
FOXP3

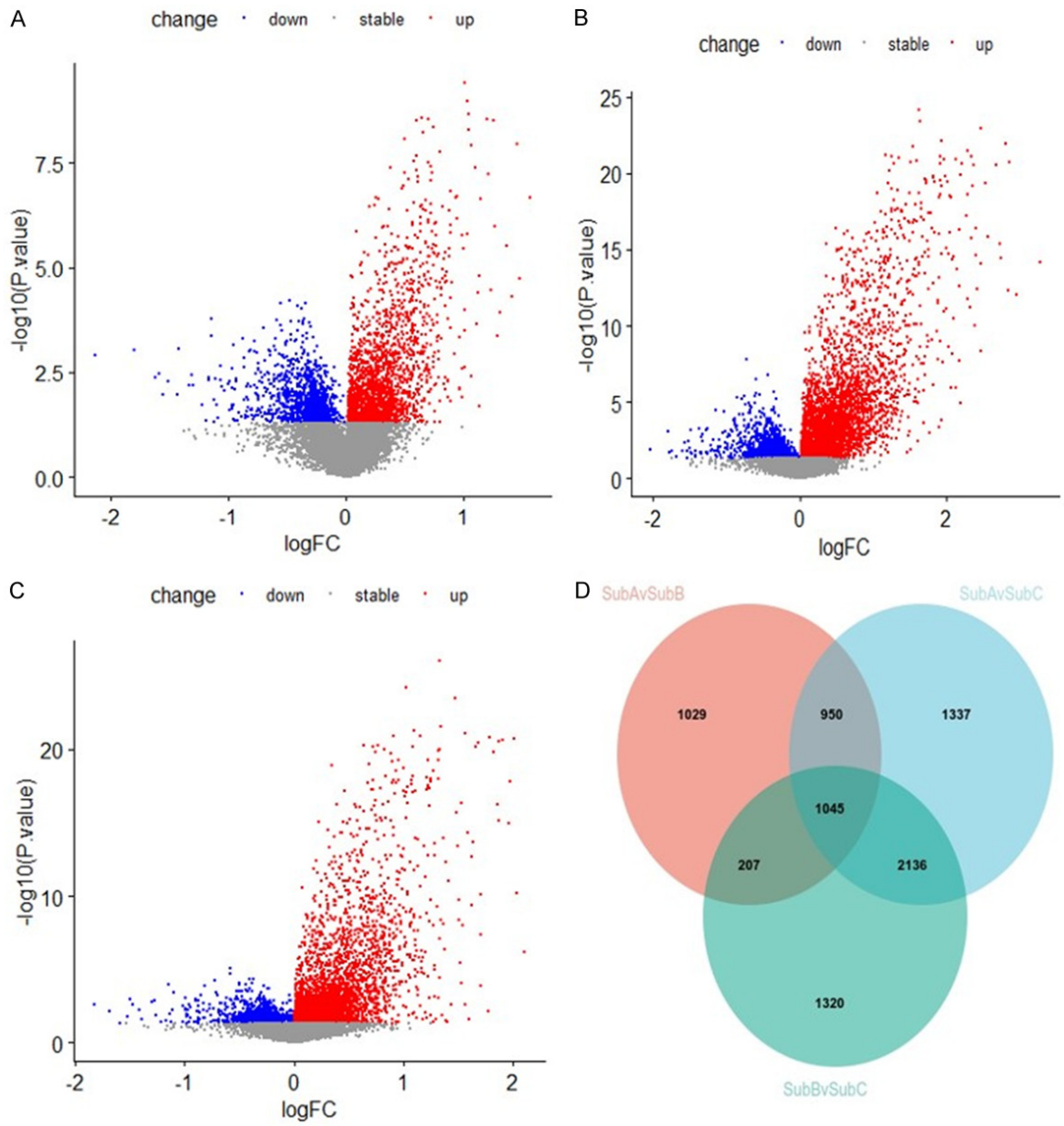

Figure S1. Differential gene screening. A. Volcanic map of differential genes in SubA & SubB. B. Volcanic map of differential genes in SubA & SubC. C. Volcanic map of differential genes in SubB & SubC. D. Venn diagram.

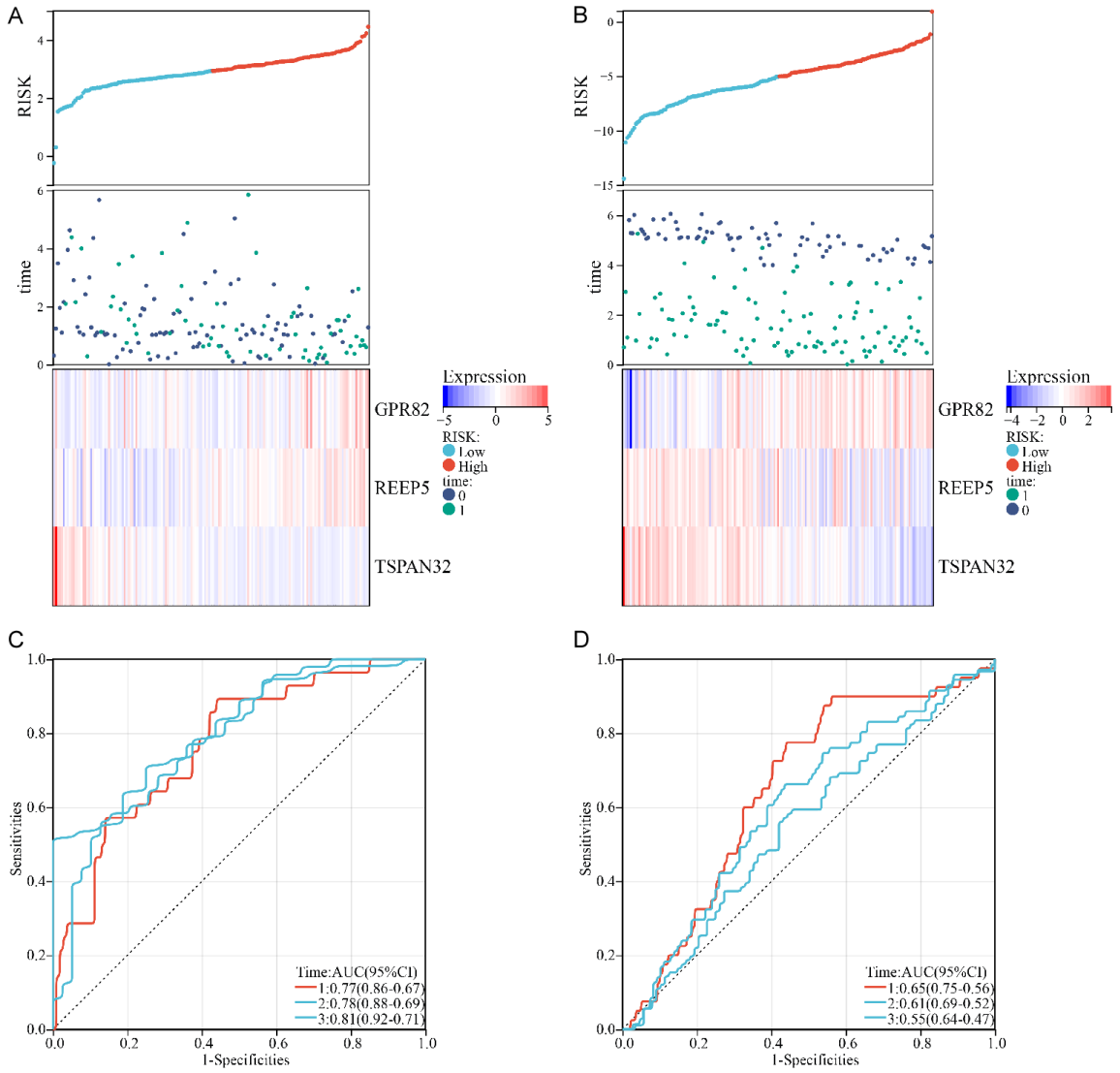

Figure S2. An overview of the risk score distribution, survival status of each patient both in the training cohort (A) and the verification cohort (B). ROC curve of the predictive value of the risk model in the training cohort (C) and validation cohort (D).

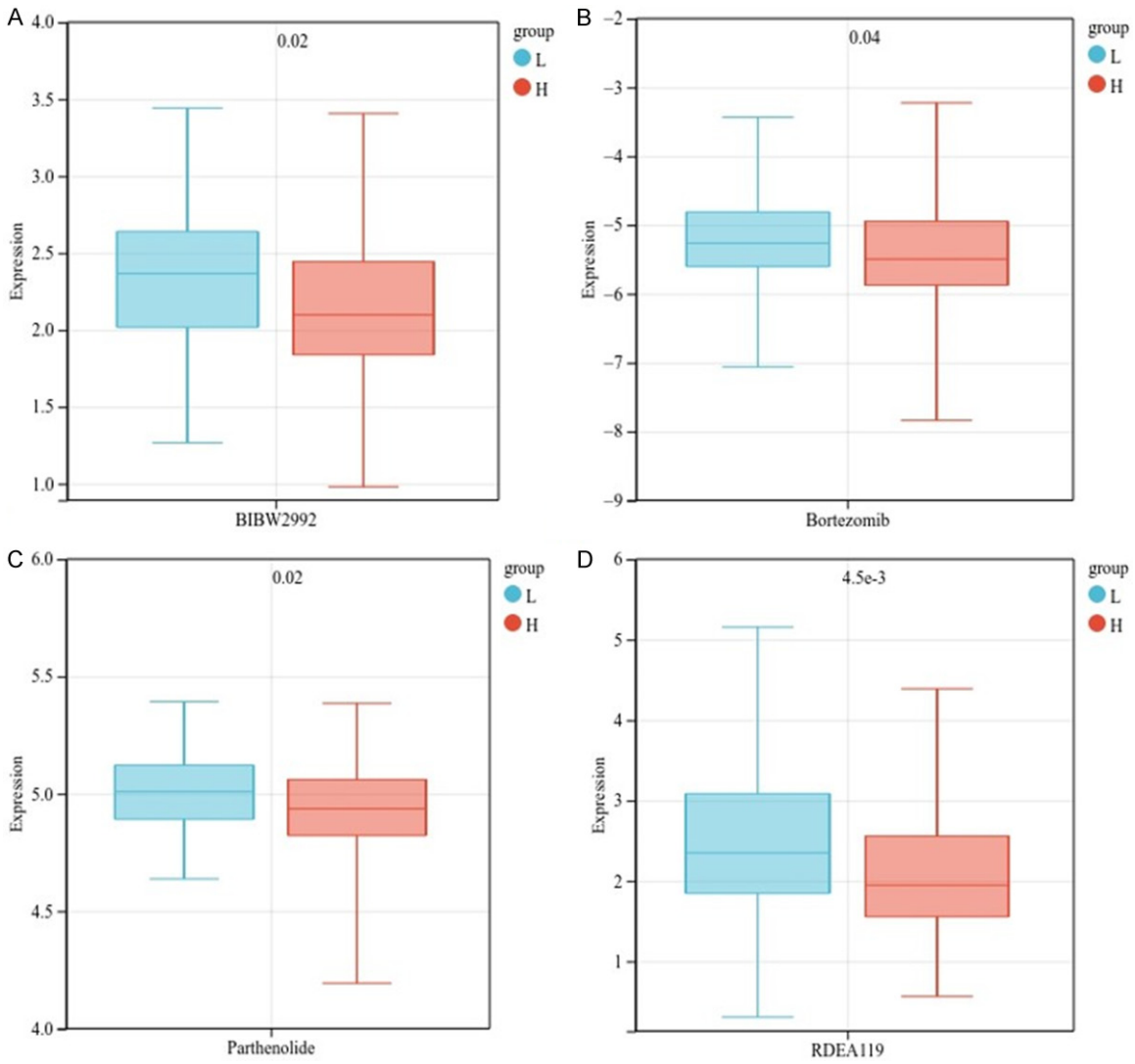

Figure S3. Targeted-drug sensitivity prediction.